

Distance dependence of the energy transfer rate from a single semiconductor nanostructure to graphene

François Federspiel,¹ Guillaume Froehlicher,¹ Michel Nasilowski,² Silvia Pedetti,² Ather Mahmood,¹ Bernard Doudin,¹ Serin Park,³ Jeong-O Lee,³ David Halley,¹ Benoît Dubertret,² Pierre Gilliot,¹ and Stéphane Berciaud^{1,*}

¹*Institut de Physique et Chimie des Matériaux de Strasbourg and NIE,
UMR 7504, Université de Strasbourg and CNRS,
23 rue du Lœss, BP43, 67034 Strasbourg Cedex 2, France*

²*Laboratoire de Physique et d'Etude des Matériaux, ESPCI-ParisTech, PSL Research University,
Sorbonne Université UPMC Univ Paris 06, CNRS, 10 rue Vauquelin 75005 Paris, France*

³*Advanced Materials Division, Korea Research Institute of Chemical Technology, Daejeon 305-343, Korea*

The near-field Coulomb interaction between a nano-emitter and a graphene monolayer results in strong Förster-type resonant energy transfer and subsequent fluorescence quenching. Here, we investigate the distance dependence of the energy transfer rate from individual, i) zero-dimensional CdSe/CdS nanocrystals and ii) two-dimensional CdSe/CdS/ZnS nanoplatelets to a graphene monolayer. For increasing distances d , the energy transfer rate from individual nanocrystals to graphene decays as $1/d^4$. In contrast, the distance dependence of the energy transfer rate from a two-dimensional nanoplatelet to graphene deviates from a simple power law, but is well described by a theoretical model, which considers a thermal distribution of free excitons in a two-dimensional quantum well. Our results show that accurate distance measurements can be performed at the single particle level using graphene-based molecular rulers and that energy transfer allows probing dimensionality effects at the nanoscale.

Keywords: graphene; semiconductor nanocrystals; quantum dots; semiconductor nanoplatelets; quantum wells; resonant energy transfer; FRET; single molecule luminescence; heterostructures; dimensionality

Introduction Graphene and colloidal semiconductor nanostructures are model low-dimensional systems, which hold promise for opto-electronic applications [1–3]. On the one hand, graphene, as a quasi-transparent semi-metal [4, 5] with excellent transport properties [6], can be seen as an ultimate transparent electrode [7, 8]. On the other hand, CSNs, in the form of zero-dimensional nanocrystals [9] (NCs or quantum dots), one-dimensional quantum rods [10] and two dimensional nanoplatelets [4, 12] (NPs, or quantum wells), are very efficient broadband light harvesting systems and size tunable nano-emitters, which are intensively used in a new generation of light emitting diodes, solar cells and photovoltaic devices [3].

There is a growing interest in combining graphene and colloidal semiconductor nanostructures in the form of hybrid systems [13–15] and devices [16–19] with new functionalities and potentially enhanced opto-electronic properties. The photoresponse of the graphene NC-hybrid system is governed by interface and short-range phenomena, such as charge transfer and Förster-type resonant energy transfer [20] (RET) (see Figure 1). While photo-induced charge transfer may result in a photogating effect and improved photogain [16, 17], energy transfer from a photoexcited colloidal semiconductor nanostructure (donor) to a graphene layer (acceptor) may efficiently generate electron-hole pairs in graphene, which is of interest for optoelectronics [2]. Importantly, graphene stands out as a uniquely tunable acceptor system, in which distinct regimes of RET can be observed by varying its Fermi level [21–24].

Highly efficient RET from individual CdSe/ZnS NCs

to graphene, resulting in a quenching of the luminescence signal by more than one order of magnitude, has recently been reported [13]. Related effects have been observed using other types of semiconductor nanostructures [14, 15, 25–27], fluorescent molecules [28–30] or NV centers [31, 32]. The observation of robust and efficient RET to graphene has stimulated numerous applications in biosensing [33] and holds promise for distance sensing [34] and photodetection. The case of a single colloidal semiconductor nanostructure near a single layer of graphene is of particular interest, since it provides a well-defined and technologically relevant system, in which the sensitivity of the RET rate to the local environment and its distance dependence can be assessed with accuracy. In addition, RET is known to be strongly affected by exciton dimensionality and exciton localization [35, 36]. Colloidal semiconductor nanostructures offer natural ways to explore such effects.

Here, we investigate RET from i) individual core/shell CdSe/CdS NCs and ii) core/shell CdSe/CdS/ZnS NPs to a graphene monolayer. Using molecular beam epitaxy, we are able to deposit ultrasmooth dielectric spacers of magnesium oxide (MgO), with variable thickness, between graphene and the nanoemitters [6]. The scaling of the RET rate with the distance d separating graphene from the nanoemitters is then quantitatively determined from the luminescence decays recorded on a collection of individual emitters. In the case of zero-dimensional NCs, the RET rate scales as $1/d^4$, as expected theoretically [21, 22, 30, 38–40]. Interestingly, although the RET rate of individual two-dimensional NPs adsorbed

on bare graphene is similar to that observed with zero-dimensional NCs, we find that the RET rate decays less rapidly with increasing distance. Such a behavior is discussed within the framework of energy transfer from free two-dimensional excitons [41, 42] to a two-dimensional acceptor.

Methods We have investigated individual colloidal semiconductor nanostructures near a graphene monolayer at room temperature, using a home-built micro-photoluminescence (PL) setup equipped with a $100\times$ (NA = 0.90) air objective. Core/shell CdSe/CdS NCs ((9.5 ± 1.5) nm in diameter, with peak emission at $\lambda_0 = 580$ nm, *i.e.*, photon energy of 2.14 eV), coated with oleylamine and oleic acid ligands, and core/shell/shell CdSe/CdS/ZnS NPs (4 monolayer thick core, ~ 1.3 nm thick shell, ~ 9 nm width, ~ 22 nm length and peak emission at $\lambda_0 = 645$ nm, *i.e.*, photon energy of 1.92 eV), coated with oleate ligands, were synthesized following previous works [2, 3, 12, 45, 46] (see also Supporting Information). Using core/shell structures dramatically reduces the possibility of irreversible photoinduced NC or NP ionization and subsequent charge transfer to graphene [46, 47]. NCs and NPs, dispersed at very low concentration into a 90%/10% hexane/octane mixture were then dropcast onto graphene samples.

Measurements on bare graphene (see Figures 1–3) were performed using mechanically exfoliated graphene monolayers deposited on transparent fused quartz substrates. The distance dependence of the energy transfer rate was investigated using large area graphene monolayers, grown by low-pressure chemical vapor deposition (LPCVD) on a copper foil, then transferred onto a fused quartz substrate using standard methods [5] (see Supporting Information). In order to vary the distance between graphene and the nano emitters, thin films of MgO were grown on top of graphene in a staircase fashion in a molecular beam epitaxy (MBE) chamber [6] before deposition of NCs or NPs. We checked by atomic force microscopy that the roughness of the MgO layer is on the order of 0.5 nm [49].

The bare graphene and graphene/MgO samples were characterized using a home-built micro-Raman setup (see Supporting Information). Although residual doping on the order of a few 10^{12} cm^{-2} could be observed, the resulting Fermi level shifts relative to the Dirac point are about one order of magnitude smaller than the energy of the emitted photons. Therefore, graphene will be considered as quasi-neutral in the following.

Individual NCs and NPs were excited using a pulsed supercontinuum laser, with a repetition rate tunable from 1.95 MHz up to 78 MHz. The unpolarized output of the supercontinuum laser at a wavelength of 480 nm (photon energy of 2.53 eV) was selected using an acousto-optic tunable filter. The full width at half maximum of the filtered pulses was ≈ 50 ps. Wide field PL images were recorded using an electron-

multiplying charge coupled device camera (emCCD). PL time traces and PL decays of individual colloidal semiconductor nanostructures were measured in a confocal arrangement, using an avalanche photodiode coupled to a time-tagged, time-correlated single photon counting board. PL spectra were recorded using a monochromator coupled to a CCD matrix. A pulse fluence lower than 1×10^{13} photons/pulse/ cm^2 at $\lambda = 480$ nm was used for all measurements. Considering similar absorption cross sections of a few 10^{-14} cm^2 for our individual NCs and NPs at 480 nm [50–52], we can estimate that on average, significantly less than one exciton per incoming laser pulse is formed in an individual NC or NP. We further verified that the PL decays of individual NCs and NPs are independent on the pulse fluence, in the range ($\approx 10^{12} - 3 \times 10^{13}$ photons/pulse/ cm^2).

Energy transfer on bare graphene Figure 1 shows wide-field PL images of individual CdSe/CdS/ZnS NPs deposited on a bare, mechanically exfoliated graphene monolayer. The PL intensity is strongly quenched, by more than one order of magnitude for NPs deposited on graphene. Very similar results were obtained using CdSe/CdS NCs. As previously discussed for individual core/shell CdSe/ZnS NCs [13], we attribute PL quenching to Förster-type RET.

We then compare the typical PL spectrum, PL time trace and PL decay of individual NCs (see Figure 2) and NPs (see Figure 3), measured on a fused quartz substrate and on a bare graphene monolayer. For each nanoemitter investigated, we introduce the average number of emitted photons per incoming laser pulse N_{em} (see PL time traces in Figures 2b,e and 3b,e). First, we note that although the peak energy of the PL spectra exhibits a slight dispersion over a collection of nanoemitters, we did not observe systematic spectral shifts for NCs or NPs on graphene with respect to a reference on fused quartz. In both cases, the PL count rates on graphene and fused quartz are similar, but the PL signals are obtained using very different repetition rates (compare Figures 2b and 2e, and Figure 3b and in Figure 3e, for NCs and NPs, respectively). On these selected examples, N_{em} is quenched by a factor of approximately 50 (60) when the NC (NP) is adsorbed on graphene, as compared to a reference recorded on fused quartz. Over time scales larger than 100 ms, we also observe, in agreement with previous observations [13, 14] that the blinking behavior, characteristic of NCs and NPs deposited on fused quartz, is seemingly reduced when the nanoemitters are adsorbed on graphene. This observation is presumably due to the acceleration of the excited state decay, which occurs before charge carriers may be trapped and allow the observation of dark and/or grey states [46, 53–56].

We now compare the PL decays of individual NCs and NPs measured on fused quartz and on graphene. Examples are shown in Figures 2c and 2f for individual NCs and in Figures 3c and 3f, for individual NPs, respec-

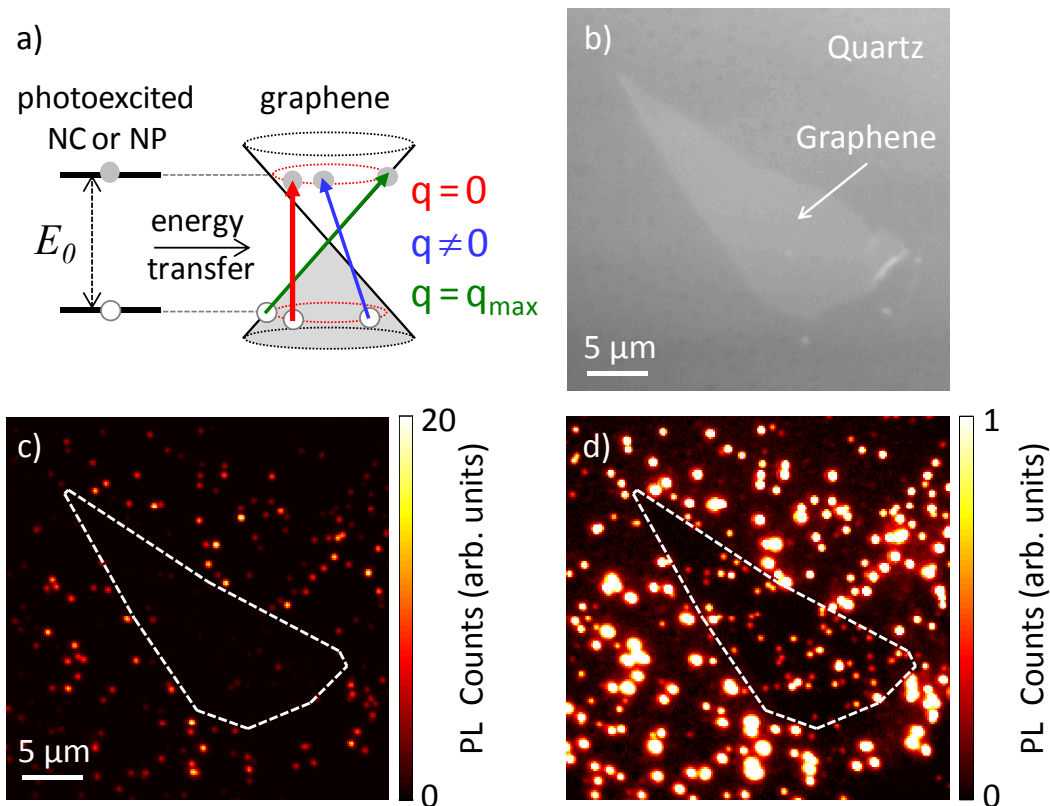


Figure 1. a) Schematic representation of the resonant energy transfer process between a photoexcited nanoemitter and undoped graphene. Electronic excitations in graphene with various transferred momenta q are shown with colored arrows. b) Optical image of an exfoliated graphene sample deposited on fused quartz. c-d) Photoluminescence (PL) image of the same sample, covered with CdSe/CdS/ZnS nanoplatelets, shown with two different linear scales of PL intensity.

tively. At this point, let us note that the room temperature typical PL decay of a single NC or NP is not mono-exponential [46, 54–56]. In the case of NCs, we found that most decays could be well fit to a bi-exponential form, while a stretched exponential form was providing better fits in the case of NPs. These complex behaviors are attributed to the existence of a distribution of bright, grey and dark states with distinct lifetimes [46, 53–56]. The fractional weight of these states in a measured decay may vary significantly from particle to particle, reflecting heterogeneities in core and shell passivation. In order to provide a general definition, the measured PL decay rate γ is defined as the maximum number of recorded counts divided by the (background corrected) total area of the PL decay. The resulting values are then multiplied by a correction factor, which takes into account the minor contribution of the instrument response function (see Figures 2c,f, Figures 3c,f, and Supporting Information). We have verified that our conclusions are independent of the method used to define the PL decay rate. For the individual NC (NP) considered here, we find that γ is enhanced by a factor of approximately 50 (80). Remarkably, the quenching factors estimated from the PL time traces are

in good agreement with the enhancement factors of the PL decay rate. This suggests that the strong PL quenching is solely due to an increase of the non-radiative decay rate, and that possible modifications of the radiative decay rate of an individual NC or NP adsorbed on graphene can be neglected. This is consistent with recent theoretical calculations, which demonstrated that the radiative lifetime of an individual emitter is marginally modified in the vicinity of graphene [22]. Thus, in the following, we will consider that $\gamma \approx \gamma_t + \gamma_0$, where γ_t is the RET rate and γ_0 is the reference decay rate measured in the absence of graphene.

Similar measurements were repeated on more than 100 NCs and NPs deposited on bare graphene. We found similar statistically averaged quenching factors of approximately 50 for NCs and NPs. Overall, for 95 % of the investigated single NCs and NPs, the RET efficiency, defined as $\eta = 1 - \gamma/\gamma_0$ is found to be larger than 95 %.

Distance dependence of the RET rate We have measured the PL decay of NCs and NPs separated from a graphene monolayer by a MgO thin film, with a thickness ranging from a few Å up to several tens of nanometers. In these experiments, the reference decay rate γ_0

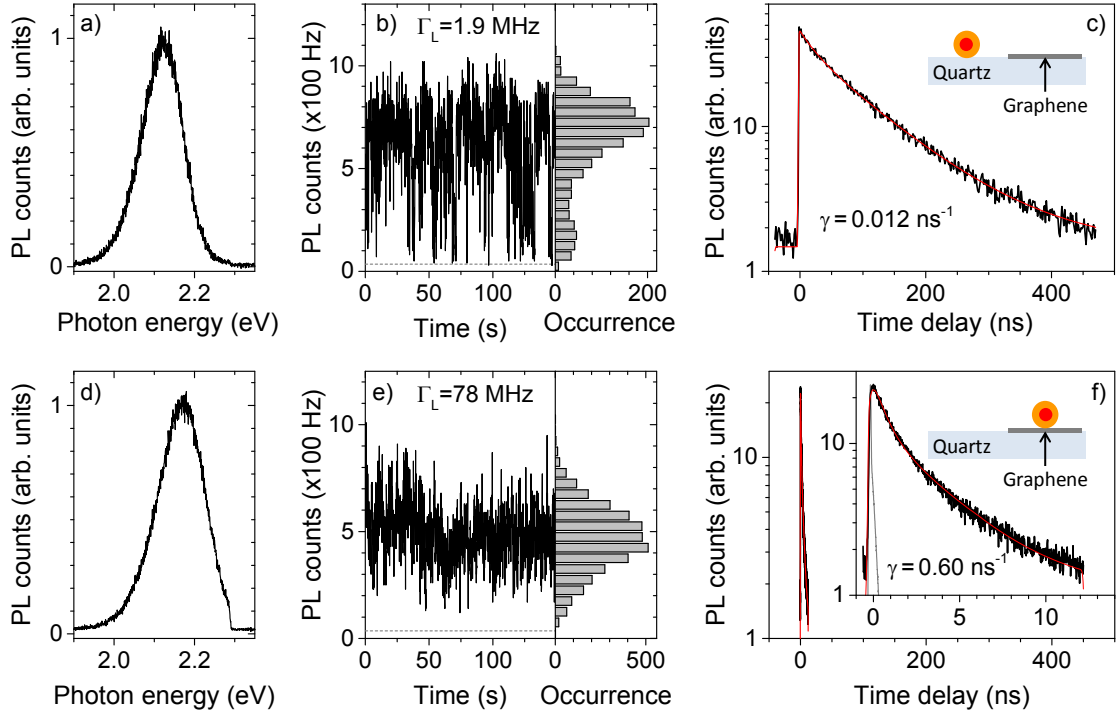


Figure 2. a-c) Photoluminescence (PL) spectrum, PL time trace and PL decay of individual CdSe/CdS nanocrystal deposited on fused quartz. d-f) Same measurements recorded on an another individual CdSe/CdS nanocrystal deposited on a graphene monolayer. All data were collected using a pulsed laser excitation, with a repetition rate Γ_L indicated in panels b) and e). The red lines in c) and f) are fits based on bi-exponential functions convoluted with the instrument response function (displayed as a gray line in f).

is the statistically averaged decay rate of NCs and NPs measured on a bare > 100 nm thick film of MgO. The results for NCs and NPs are summarized in Figures 4 and 5, respectively. Each point corresponds to a statistical average over 10 to 30 single NCs, and over more than 25 single NPs, respectively. The vertical error bars correspond to the standard deviations, while the horizontal error bars account for the roughness of the MgO film. For both NC and NPs, we observe that the measured decay rate decreases significantly, when increasing the thickness of the MgO film. However, as shown in figures 4c and 5c, the product $N_{em}\gamma$ varies by less than a factor of 2 and, considering the standard deviations associated with each distribution, can be considered as constant. This generalizes the conclusions drawn from the analysis of Figures 2 and 3.

A key observation is that the decrease of the PL decay rate as function of the MgO thickness is seemingly steeper for NCs than for NPs (see also Figure 7 in the Supporting Information for a comparison of the normalized decay rates). This points towards the effect of dimensionality on RET, which we now discuss. Let us first focus on the case of NCs interacting with graphene. Based on the well known $1/d^6$ distance dependence of the Förster energy transfer rate between two point-like dipoles [20],

one would expect the measured decay rate to scale as

$$\gamma = \gamma_0 \left[1 + \left(\frac{z_0}{d_0 + d_{MgO}} \right)^p \right], \quad (1)$$

where the distance d separating the nanoemitter from the graphene layer is $d = d_0 + d_{MgO}$, with d_{MgO} , the thickness of the MgO film and d_0 , the minimal distance between the center of the nanoemitter and the graphene surface in the absence of a MgO spacer, where z_0 characterizes the RET efficiency, and p is related to the dimensionality of the donor and acceptor. A straightforward extension of Förster's theory would then give $p = 4$ for a zero-dimensional emitter interacting with a two-dimensional assembly of independent dipoles [38, 39]. Indeed, for NCs (see Fig. 4b, using $p = 4$, we obtain a good fit with $z_0 = (11.5 \pm 1.5)$ nm and $d_0 = (5.5 \pm 1)$ nm. The latter value is slightly larger than the average physical radius of the NCs, which is consistent with a possible contribution from the surrounding ligands and residual adsorbates to d_0 .

Although a fit based on Eq.1 is in good agreement with our measurements, one has to recall that Eq.1 overlooks the fact that graphene is a two-dimensional system with extended, delocalized electronic wavefunctions and a well defined electronic dispersion. The RET rate γ_t^{0D} from a

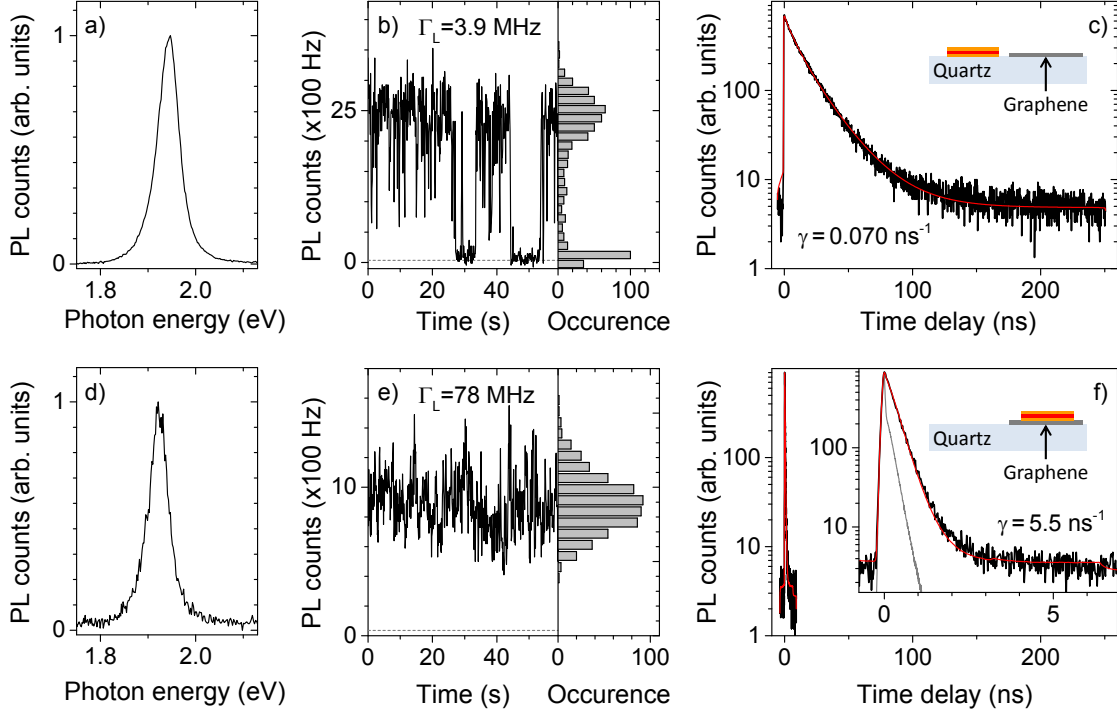


Figure 3. a-c) Photoluminescence (PL) spectrum, PL time trace and PL decay of an individual CdSe/CdS/ZnS nanoplatelet deposited on fused quartz. d-f) Same measurements on another individual CdSe/CdS/ZnS nanoplatelet deposited on a graphene monolayer. All data were collected using a pulsed laser excitation, with a repetition rate Γ_L indicated in panels b) and e). The red lines in c) and f) are fits based on stretched exponential functions convoluted with the instrument response function (displayed as a gray line in f).

single point-like dipole to graphene has been extensively studied theoretically in recent years [21, 22, 30, 40, 57, 58] and can be written as [22, 40]

$$\gamma_t^{0D} \propto \int_0^{q_{\max}} \frac{dq q^3 e^{-2qd}}{\sqrt{q_{\max}^2 - q^2}}, \quad (2)$$

where q is the transferred momentum, $q_{\max} = \frac{2\pi c}{\lambda_0 v_F}$ is the largest transferable momentum, λ_0 is the wavelength of the emitted photons, c is the speed of light and $v_F \approx 1.1 \times 10^6$ m/s is the Fermi velocity in graphene. Contrary to far-field emission and absorption processes, the RET process described by Eq.2 involves a finite momentum transfer (see Figure 1a), which is on the order of $1/d$. For neutral graphene, and distances such that $d \gg 1/q_{\max} \approx 0.3$ nm, the denominator of the integrand in Eq.2, which originates from the (momentum dependent) optical conductivity of graphene [22], only gives significant contributions for $q \ll q_{\max}$ (quasi-vertical transitions), and can thus be approximated as a constant. In these conditions, graphene can be treated as a two-dimensional assembly of incoherent point-like dipoles, and Eq.2 simplifies as $\gamma_t^{0D} \approx \gamma_0 \left(\frac{z_0}{d}\right)^4$. Nevertheless, it must be emphasized that Eq. 2 applies to a

point-like donor, while in our case, the NCs have a finite radius, larger than the thinnest MgO films (0.6 nm) deposited here. However, the surrounding ligands and the finite thickness of the CdS shell of our CdSe/CdS NCs warrant that there is a minimal distance of a few nanometers between the graphene layer and the emitting CdSe core. We will therefore consider that the *long distance* approximation is valid and neglect the finite size of the NCs and NPs. Considering random relative dipole orientation, we obtain [40] $z_0^4 = \frac{3\alpha}{2048 \pi^3 F^2 \varepsilon^{5/2}} \lambda_0^4$, where $\alpha \approx 1/137$ is the fine structure constant, ε is the effective dielectric constant (at λ_0) of the surrounding medium and $F = \frac{3\varepsilon}{\varepsilon_{\text{CdS}} + 2\varepsilon}$ is a screening factor [59]. Using $\varepsilon \approx (\varepsilon_{\text{MgO}} + 1)/2 \approx 2$ results in $z_0 \approx 11$ nm, in good agreement with our measurements.

We now address the distance dependence of the RET rate from single NPs to graphene. The NPs cores are atomically smooth and have recently been shown to behave as genuine quantum wells [12]. As a result, a different regime of RET is anticipated when a two-dimensional donor is involved. Electronic states in NPs are described by extended wave functions that are coherent over large distances in the NP plane. However, at finite temperature, one has to consider, in a photoexcited NP, a thermal distribution of excitons with different in-plane cen-

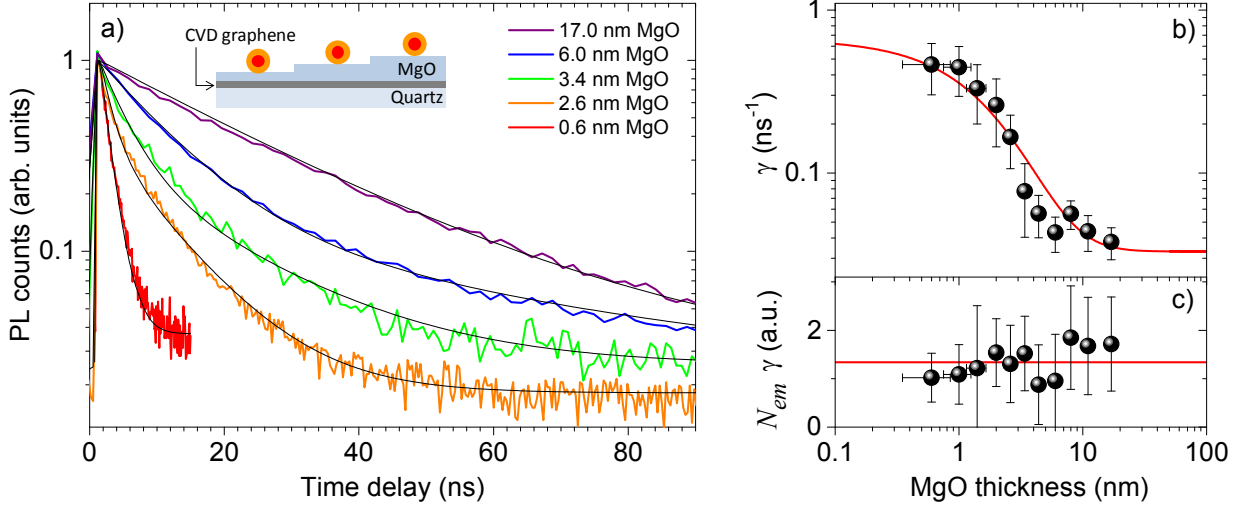


Figure 4. a) Selected luminescence decays of individual CdSe/CdS nanocrystals separated from graphene by a MgO spacer graphene with increasing thicknesses. The thin black lines are fits based on bi-exponential decays convoluted with the instrument response function. b) Statistically averaged measured decay rate γ as a function of the thicknesses of the MgO spacer. The red solid line is a fit based on Eq. 1, with $p = 4$, $d_0 = 5.5$ nm, $z_0 = 11.5$ nm. c) Statistically averaged product of the number of emitted photons per exciting laser pulse N_{em} and the decay rate γ .

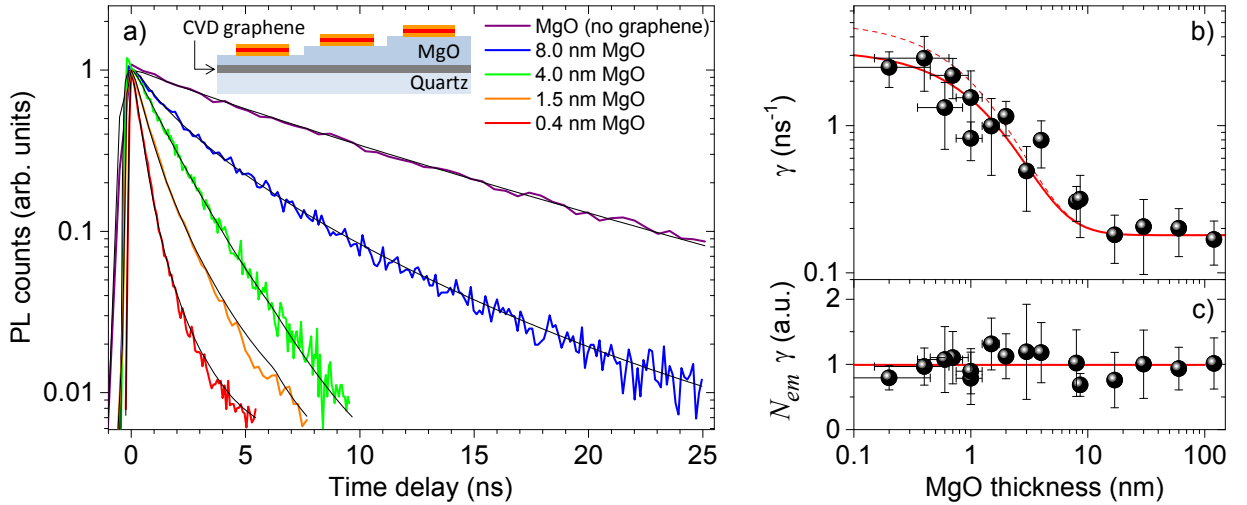


Figure 5. a) Selected luminescence decays of individual CdSe/CdS/ZnS nanoplatelets separated from graphene by a MgO spacer graphene with increasing thicknesses. The thin black lines are fits based on stretched exponential decays convoluted with the instrument response function. b) Statistically averaged measured decay rate γ as a function of the thicknesses of the MgO spacer. The red solid and dashed lines are fits based on Eq. 3, with $d_0 = 3.5$ nm, $\Lambda = 7.5$ nm, and on Eq. 1 with $p = 4$, $d_0 = 3.5$ nm, $z_0 = 8.0$ nm, respectively. c) Statistically averaged product of the number of emitted photons per exciting laser pulse N_{em} and the decay rate γ .

ter of mass momentum. Besides, since the thickness of the NP shell is on the order of 2 nm, there is a minimal separation between the NP core and graphene, such that the approximation $d \gg 1/q_{max}$ holds (*i.e.*, graphene can also be treated as an incoherent plane of point-like-dipoles). Similar situations have been previously modeled by Basko *et al.* [41] and Kos *et al.* [42] for hybrid

systems composed of quantum wells transferring energy to an assembly (thick film or monolayer) of point-like dipoles. The calculated RET rate writes

$$\gamma_t^{2D}(d) \propto \int_0^\infty dq q^3 e^{-2qd} e^{-\left(\frac{\Lambda q}{2\pi}\right)^2}, \quad (3)$$

where $\Lambda = \frac{h}{\sqrt{2m^*k_B T}}$ is the de Broglie thermal length,

with h the Planck constant, k_B the Boltzmann constant and m^* the mass of the lowest energy heavy hole exciton ($m^* \approx m_e$, where m_e is the free electron mass) in CdSe [12, 60].

This expression applies to free excitons in an infinite quantum well, with thickness ($L_z \ll d$). The assumption of free excitons is consistent with the reported low density of trapping sites of CdSe-based core/shell NPs [46]. In addition, since the typical lateral dimensions of our NPs ($L_x = (22 \pm 2)$ nm and $L_y = (9 \pm 1.5)$ nm) exceed Λ (at room temperature, $\Lambda \approx 7.5$ nm), finite size effects can be neglected. We have thus attempted to fit the data in Figure 5b using the expression $\gamma(d) = \gamma_0 + \gamma_t^{2D}(d)$. A good agreement with our experimental results is obtained using $d_0 = (3.5 \pm 1)$ nm. Again, the latter value is consistent with the thickness of the core and shell of the NPs and includes a minor contribution from the surrounding ligands and residual adsorbates.

An analysis of the limiting cases of Eq. 3 provides a rationale for the observed scaling. In the short distance limit, $d \ll \Lambda$, γ_t^{2D} becomes independent on the distance and is determined by the thermal cutoff. In contrast, in the large distance (or high temperature) limit, $d \gg \Lambda$ and γ_t^{2D} follows a $1/d^4$ scaling, as expected in the case of a two-dimensional assembly of incoherent point-like dipoles. Since, at room temperature, Λ falls exactly in our measurement range, we expect the RET rate to decay more smoothly than $1/d^4$ for $d < \Lambda$. This is indeed observed experimentally (see Fig 5b), since a scaling based on Eq. 2, with $p = 4$ and $d_0 = 3.5$ nm, having asymptotic behavior for large d as our fit based on Eq. 3, would predict a higher γ in the short distance limit.

The results shown in Figure 5 suggest that even at room temperature, the distance scaling of the RET rate from an extended donor (such as a two-dimensional NP) to graphene exhibits, as expected theoretically, a slight deviation from a simple power law. Following Eq.3, this deviation is expected to be more prominent at lower temperatures. Thus, further investigations of the distance and temperature dependence of the RET rate for various NP architectures could provide insights into the dimensionality of excitons in these novel systems [36].

In conclusion, Förster-type resonant energy transfer dramatically affects the photophysics of semiconductor nanostructures absorbed on graphene. In spite of its atomic thinness, a single layer of graphene typically quenches more than 95% of the luminescence of individual nanocrystals or nanoplatelets. The observation of well-defined distance scalings of the resonant energy transfer rate suggests that novel graphene-based molecular rulers can be engineered using semiconductor nanostructures with different size, shape, and dimensionality. This is a promising development, especially for biological research. Finally, with the prospect of designing hybrid opto-electronic devices, we show that graphene can very efficiently harvest energy from photoexcited semiconduc-

tor nanostructures, which is of interest for photodetection. A major challenge is now to dissociate the electron-hole excitations generated in graphene before their fast relaxation into heat [61, 62].

Acknowledgement We are grateful to D.M. Basko and G. Weick for fruitful discussions, to R. Bernard, S. Siegwald and H. Majjad for help with sample fabrication and characterization in the STNano clean room facility, and to M. Romeo for technical support. The authors at IPCMS acknowledge financial support from the CNRS, Université de Strasbourg, C’Nano GE and the Agence Nationale de Recherche (ANR) under grants QuandDoGra ANR-12-JS10-0001 and Fungraph ANR-11-IS10-0003. B.D. (at ESPCI) thanks the ANR for funding under grants SNAP and QDOTICS. J-O. L. (at KRICT) acknowledges support from NRF-ANR program through the National Research Foundation of Korea funded by the Ministry of education, Science and Technology (NRF-2011-K2A1A5-2011-0031552).

Supporting Information Synthesis and characterization of CdSe/CdS nanocrystals and CdSe/CdS/ZnS nanoplatelets, graphene growth by chemical vapor deposition, sample characterization by micro-Raman spectroscopy, definition of the energy transfer rate, comparison of the normalized distance dependent decay rates.

* stephane.berciaud@ipcms.unistra.fr

- [1] F. Bonaccorso, Z. Sun, T. Hasan, and A. C. Ferrari, “Graphene photonics and optoelectronics,” *Nature Photonics* **4**, 611–622 (2010).
- [2] F. H. L. Koppens, T. Mueller, Ph Avouris, A. C. Ferrari, M. S. Vitiello, and M. Polini, “Photodetectors based on graphene, other two-dimensional materials and hybrid systems,” *Nature Nanotechnology* **9**, 780–793 (2014).
- [3] Dmitri V. Talapin, Jong-Soo Lee, Maksym V. Kovalenko, and Elena V. Shevchenko, “Prospects of colloidal nanocrystals for electronic and optoelectronic applications,” *Chemical Reviews* **110**, 389–458 (2010).
- [4] R. R. Nair, P. Blake, A. N. Grigorenko, K. S. Novoselov, T. J. Booth, T. Stauber, N. M. R. Peres, and A. K. Geim, “Fine Structure Constant Defines Visual Transparency of Graphene,” *Science* **320**, 1308 (2008).
- [5] Kin Fai Mak, Matthew Y. Sfeir, Yang Wu, Chun Hung Lui, James A. Misewich, and Tony F. Heinz, “Measurement of the optical conductivity of graphene,” *Physical Review Letters* **101**, 196405 (2008).
- [6] S. Das Sarma, Shaffique Adam, E. H. Hwang, and Enrico Rossi, “Electronic transport in two-dimensional graphene,” *Review of Modern Physics* **83**, 407–470 (2011).
- [7] Xuan Wang, Linjie Zhi, and Klaus Mllen, “Transparent, conductive graphene electrodes for dye-sensitized solar cells,” *Nano Letters* **8**, 323 (2008).
- [8] Keun Soo Kim, Yue Zhao, Houk Jang, Sang Yoon Lee, Jong Min Kim, Kwang S. Kim, Jong-Hyun Ahn, Philip Kim, Jae-Young Choi, and Byung Hee Hong, “Large-scale pattern growth of graphene films for stretchable transparent electrodes,” *Nature* **457**, 706–710 (2009).

- [9] V.I. Edited by Klimov, *Nanocrystal Quantum Dots* (CRC Press, UK, 2010).
- [10] Xiaogang Peng, Liberato Manna, Weidong Yang, Juanita Wickham, Erik Scher, Andreas Kadavanich, and A. P. Alivisatos, "Shape control of CdSe nanocrystals," *Nature* **404**, 59–61 (2000).
- [4] Sandrine Ithurria and Benoit Dubertret, "Quasi 2D colloidal CdSe platelets with thicknesses controlled at the atomic level," *Journal of the American Chemical Society* **130**, 16504–16505 (2008).
- [12] S. Ithurria, M. D. Tessier, B. Mahler, R. P. S. M. Lobo, B. Dubertret, and Al L. Efros, "Colloidal nanoplatelets with two-dimensional electronic structure," *Nature Materials* **10**, 936–941 (2011).
- [13] Zheyuan Chen, Ste?phane Berciaud, Colin Nuckolls, Tony F. Heinz, and Louis E. Brus, "Energy transfer from individual semiconductor nanocrystals to graphene," *ACS Nano* **4**, 2964–2968 (2010).
- [14] O. A. Ajayi, N. C. Anderson, M. Cotlet, N. Petrone, T. Gu, A. Wolcott, F. Gesuele, J. Hone, J. S. Owen, and C. W. Wong, "Time-resolved energy transfer from single chloride-terminated nanocrystals to graphene," *Applied Physics Letters* **104**, 171101 (2014).
- [15] Benoît Rogez, Heejun Yang, Eric Le Moal, Sandrine Lévêque-Fort, Elizabeth Boer-Duchemin, Fei Yao, Young-Hee Lee, Yang Zhang, K. David Wegner, Niko Hildebrandt, Andrew Mayne, and Gérald Dujardin, "Fluorescence lifetime and blinking of individual semiconductor nanocrystals on graphene," *The Journal of Physical Chemistry C* **118**, 18445–18452 (2014).
- [16] Gerasimos Konstantatos, Michela Badioli, Louis Gaudreau, Johann Osmond, Maria Bernechea, F. Pelayo Garcia de Arquer, Fabio Gatti, and Frank H. L. Koppens, "Hybrid graphene-quantum dot phototransistors with ultrahigh gain," *Nature Nanotechnology* **7**, 363 (2012).
- [17] Zhenhua Sun, Zhike Liu, Jinhua Li, Guo-an Tai, Shu-Ping Lau, and Feng Yan, "Infrared photodetectors based on cvd-grown graphene and pbs quantum dots with ultrahigh responsivity," *Advanced Materials* **24**, 5878 (2012).
- [18] Alexander V. Klekachev, Inge Asselberghs, Sergey N. Kuznetsov, Mirco Cantoro, Jeong Hun Mun, Byung-Jin Cho, Jun-ichi Hotta, Johan Hofkens, Marleen van der Veen, Andr L. Stesmans, Marc M. Heyns, and Stefan De Gendt, "Charge transfer effects in graphene-cdse/zns quantum dots composites," *Proc. SPIE* **8462**, 84620L (2012).
- [19] Alexander V. Klekachev, Sergey N. Kuznetsov, Inge Asselberghs, Mirco Cantoro, Jeong Hun Mun, Byung Jin Cho, André L. Stesmans, Marc M. Heyns, and Stefan De Gendt, "Graphene as anode electrode for colloidal quantum dots based light emitting diodes," *Applied Physics Letters* **103**, 043124 (2013).
- [20] Th Förster, "Zwischenmolekulare energiewanderung und fluoreszenz," *Annalen der physik* **437**, 55 (1948).
- [21] Kirill A. Velizhanin and Anatoly Efimov, "Probing plasmons in graphene by resonance energy transfer," *Phys. Rev. B* **84**, 085401 (2011).
- [22] G. Gmez-Santos and T. Stauber, "Fluorescence quenching in graphene: A fundamental ruler and evidence for transverse plasmons," *Phys. Rev. B* **84**, 165438 (2011).
- [23] K. J. Tielrooij, L. Orona, A. Ferrier, M. Badioli, G. Navickaite, S. Coop, S. Nanot, B. Kalinic, T. Cesca, L. Gaudreau, Q. Ma, A. Centeno, A. Pesquera, A. Zurutuza, H. de Riedmatten, P. Goldner, F. J. Garcia de Abajo, P. Jarillo-Herrero, and F. H. L. Koppens, "Electrical control of optical emitter relaxation pathways enabled by graphene," arXiv:1410.1361 (2014).
- [24] Jiye Lee, Wei Bao, Long Ju, P. James Schuck, Feng Wang, and Alexander Weber-Bargioni, "Switching individual quantum dot emission through electrically controlling resonant energy transfer to graphene," *Nano Letters* **14**, 7115–7119 (2014).
- [25] Eyal Shafran, Benjamin D. Mangum, and Jordan M. Gerton, "Energy transfer from an individual quantum dot to a carbon nanotube," *Nano Letters* **10**, 4049–4054 (2010).
- [26] Sebastian Jander, Andreas Kornowski, and Horst Weller, "Energy transfer from CdSe/CdS nanorods to amorphous carbon," *Nano Letters* **11**, 5179–5183 (2011).
- [27] T. N. Lin, L. T. Huang, G. W. Shu, C. T. Yuan, J. L. Shen, C. A. J. Lin, W. H. Chang, C. H. Chiu, D. W. Lin, C. C. Lin, and H. C. Kuo, "Distance dependence of energy transfer from ingan quantum wells to graphene oxide," *Opt. Lett.* **38**, 2897–2899 (2013).
- [28] Emanuele Treossi, Manuela Melucci, Andrea Liscio, Massimo Gazzano, Paolo Samori, and Vincenzo Palermo, "High-contrast visualization of graphene oxide on dye-sensitized glass, quartz, and silicon by fluorescence quenching," *Journal of the American Chemical Society* **131**, 15576–15577 (2009).
- [29] Jaemyung Kim, Laura J. Cote, Franklin Kim, and Ji-axing Huang, "Visualizing graphene based sheets by fluorescence quenching microscopy," *Journal of the American Chemical Society* **132**, 260267 (2009).
- [30] L. Gaudreau, K. J. Tielrooij, G. E. D. K. Prawiroatmodjo, J. Osmond, F. J. Garcia de Abajo, and F. H. L. Koppens, "Universal distance-scaling of nonradiative energy transfer to graphene," *Nano Letters* **13**, 2030–2035 (2013).
- [31] Rainer J. Stöhr, Roman Kolesov, Kangwei Xia, Rolf Reuter, Jan Meijer, Gennady Logvenov, and Jörg Wrachtrup, "Super-resolution fluorescence quenching microscopy of graphene," *ACS Nano* **6**, 9175–9181 (2012).
- [32] Julia Tisler, Thomas Oeckinghaus, Rainer J. Stöhr, Roman Kolesov, Rolf Reuter, Friedemann Reinhard, and Jörg Wrachtrup, "Single defect center scanning near-field optical microscopy on graphene," *Nano Letters* **13**, 3152–3156 (2013).
- [33] Ying Wang, Zhaohui Li, Jun Wang, Jinghong Li, and Yuehe Lin, "Graphene and graphene oxide: biofunctionalization and applications in biotechnology," *Trends in Biotechnology* **29**, 205 – 212 (2011).
- [34] G Mazzamuto, A Tabani, S Pazzagli, S Rizvi, A Reserbat-Plantey, K Schädler, G Navickaite, L Gaudreau, F S Cataliotti, F Koppens, and C Toninelli, "Single-molecule study for a graphene-based nano-position sensor," *New Journal of Physics* **16**, 113007 (2014).
- [35] Shira Halivni, Amit Sitt, Ido Hadar, and Uri Banin, "Effect of nanoparticle dimensionality on fluorescence resonance energy transfer in nanoparticle-dye conjugated systems," *ACS Nano* **6**, 2758–2765 (2012).
- [36] Jan Junis Rindermann, Galia Pozina, Bo Monemar, Lars Hultman, Hiroshi Amano, and Pavlos G. Lagoudakis, "Dependence of resonance energy transfer on exciton dimensionality," *Physical Review Letters* **107**, 236805 (2011).
- [6] Florian Godel, Emmanuelle Pichonat, Dominique Vignaud, Hicham Majjad, Dominik Metten, Yves Henry,

- Stphane Berciaud, Jean-Francois Dayen, and David Haley, "Epitaxy of MgO magnetic tunnel barriers on epitaxial graphene," *Nanotechnology* **24**, 475708 (2013).
- [38] Hans Kuhn, "Classical aspects of energy transfer in molecular systems," *The Journal of Chemical Physics* **53**, 101–108 (1970).
- [39] R. R. Chance, A. Prock, and R. Silbey, "Molecular fluorescence and energy transfer near interfaces," *Adv. Chem. Phys.* **37**, 65 (1978).
- [40] R. S. Swathi and K. L. Sebastian, "Long range resonance energy transfer from a dye molecule to graphene has (distance)⁴ dependence," *The Journal of Chemical Physics* **130**, 086101 (2009).
- [41] D. M. Basko, V. M. Agranovich, F. Bassani, and G. C. La Rocca, "Energy transfer from a semiconductor quantum dot to an organic matrix," *Eur. Phys. J. B* **13**, 653–659 (2000).
- [42] S. Kos, M. Achermann, V. I. Klimov, and D. L. Smith, "Different regimes of förster-type energy transfer between an epitaxial quantum well and a proximal monolayer of semiconductor nanocrystals," *Phys. Rev. B* **71**, 205309 (2005).
- [3] Mona B. Mohamed, Dino Tonti, Awos Al-Salman, Abdelkrim Chemseddine, and Majed Chergui, "Synthesis of high quality zinc blende cdse nanocrystals," *The Journal of Physical Chemistry B* **109**, 10533–10537 (2005).
- [2] Benoit Mahler, Piernicola Spinicelli, Stéphanie Buil, Xavier Quelin, Jean-Pierre Hermier, and Benoit Dubertret, "Towards non-blinking colloidal quantumdots," *Nature Materials* **7**, 659–664 (2008).
- [45] Benoit Mahler, Brice Nadal, Cecile Bouet, Gilles Patriarche, and Benoit Dubertret, "Core/Shell colloidal semiconductor nanoplatelets," *Journal of the American Chemical Society* **134**, 18591–18598 (2012).
- [46] M. D. Tessier, B. Mahler, B. Nadal, H. Heuclin, S. Pedetti, and B. Dubertret, "Spectroscopy of colloidal semiconductor Core/Shell nanoplatelets with high quantum yield," *Nano Letters* **13**, 3321–3328 (2013).
- [47] Margaret A. Hines and Philippe Guyot-Sionnest, "Synthesis and characterization of strongly luminescing zns-capped cdse nanocrystals," *The Journal of Physical Chemistry* **100**, 468–471 (1996).
- [5] Xuesong Li, Weiwei Cai, Jinho An, Seyoung Kim, Junghyo Nah, Dongxing Yang, Richard Piner, Aruna Velamakanni, Inhwa Jung, Emanuel Tutuc, Sanjay K. Banerjee, Luigi Colombo, and Rodney S. Ruoff, "Large-area synthesis of high-quality and uniform graphene films on copper foils," *Science* **324**, 1312–1314 (2009).
- [49] W. H. Wang, W. Han, K. Pi, K. M. McCreary, F. Miao, W. Bao, C. N. Lau, and R. K. Kawakami, "Growth of atomically smooth mgo films on graphene by molecular beam epitaxy," *Applied Physics Letters* **93**, 183107 (2008).
- [50] C. A. Leatherdale, W.-K. Woo, F. V. Mikulec, and M. G. Bawendi, "On the absorption cross section of CdSe nanocrystal quantum dots," *The Journal of Physical Chemistry B* **106**, 7619–7622 (2002).
- [51] Y.-S. Park, A. V. Malko, J. Vela, Y. Chen, Y. Ghosh, F. Garcia-Santamaria, J. A. Hollingsworth, V. I. Klimov, and H. Htoon, "Near-unity quantum yields of biexciton emission from CdSe/CdS nanocrystals measured using single-particle spectroscopy," *Physical Review Letters* **106**, 187401 (2011).
- [52] Chunxing She, Igor Fedin, Dmitriy S. Dolzhenkov, Arnaud Demortire, Richard D. Schaller, Matthew Pelton, and Dmitri V. Talapin, "Low-threshold stimulated emission using colloidal quantum wells," *Nano Letters* **14**, 2772–2777 (2014).
- [53] F Cichos, C Vonborczyskowski, and M Orrit, "Power-law intermittency of single emitters," *Current Opinion in Colloid & Interface Science* **12**, 272–284 (2007).
- [54] P. Spinicelli, S. Buil, X. Quélin, B. Mahler, B. Dubertret, and J.-P. Hermier, "Bright and grey states in cdse-cds nanocrystals exhibiting strongly reduced blinking," *Physical Review Letters* **102**, 136801 (2009).
- [55] Anton V. Malko, Young-Shin Park, Siddharth Sampat, Christophe Galland, Javier Vela, Yongfen Chen, Jennifer A. Hollingsworth, Victor I. Klimov, and Han Htoon, "Pump-intensity- and shell-thickness-dependent evolution of photoluminescence blinking in individual Core/Shell CdSe/CdS nanocrystals," *Nano Letters* **11**, 5213–5218 (2011).
- [56] Mickaël D. Tessier, Clémentine Javaux, Ivan Maksimovic, Vincent Loriette, and Benoit Dubertret, "Spectroscopy of single CdSe nanoplatelets," *ACS Nano* **6**, 6751–6758 (2012).
- [57] R. S. Swathi and K. L. Sebastian, "Resonance energy transfer from a dye molecule to graphene," *The Journal of Chemical Physics* **129**, 054703 (2008).
- [58] Ermin Malic, Heiko Appel, Oliver T. Hofmann, and Angel Rubio, "Förster-induced energy transfer in functionalized graphene," *The Journal of Physical Chemistry C* **118**, 9283–9289 (2014).
- [59] Marco Califano, Alberto Franceschetti, and Alex Zunger, "Temperature dependence of excitonic radiative decay in CdSe quantum dots: The role of surface hole traps," *Nano Letters* **5**, 2360–2364 (2005).
- [60] R. Blachnik, J. Chu, R.R. Galazka, J. Geurts, J. Gutowski, B. Hönerlage, D. Hofmann, J. Kosut, R. Lévy, P. Michler, U. Neukirch, T. Story, D. Strauch, and A. Waag, "Semiconductors: Ii-vi and i-vii compounds; semimagnetic compounds," in *Landolt-Börnstein, New Series III/41B*, edited by U. Rössler (Springer Verlag, 1999).
- [61] Jens Christian Johannsen, Søren Ulstrup, Federico Cilento, Alberto Crepaldi, Michele Zacchigna, Cephise Cacho, I. C. Edmond Turcu, Emma Springate, Felix Fromm, Christian Raidel, Thomas Seyller, Fulvio Parmigiani, Marco Grioni, and Philip Hofmann, "Direct view of hot carrier dynamics in graphene," *Physical Review Letters* **111**, 027403 (2013).
- [62] Isabella Gierz, Jesse C. Petersen, Matteo Mitranò, Cephise Cacho, I. C. Edmond Turcu, Emma Springate, Alexander Stöhr, Axel Köhler, Ulrich Starke, and Andrea Cavalleri, "Snapshots of non-equilibrium dirac carrier distributions in graphene," *Nature Materials* **12**, 1119–1124 (2013).

Supporting Information

SYNTHESIS OF CdSe/ CdS NANOCRYSTALS

Chemicals: 1-Octadecene (ODE, 90 %, Aldrich), oleylamine (OLA, 70 %, Fluka), oleic acid (OA, 90 %, Aldrich), sodium myristate (99 %, Fluka), cadmium oxide (99.99 %, Aldrich), selenium powder 100 mesh (99.99 %, Aldrich), sulfur (99.998 %, Aldrich), trioctylphosphine (TOP, 90 %, Cytec) and tetradecylphosphonic acid (TDPA, 97 %, PCI synthesis) were used as received.

Precursors preparation: Cadmium myristate was prepared according to ref. [1]. The solution of cadmium oleate 0.5 M in oleic acid was synthesized by heating 6.42 g of CdO in 100 mL of oleic acid at 160 °C under argon until it turned colorless. The solution was then degassed under vacuum at 100 °C for 1 hour. Sulfur stock solution in ODE (S-ODE 0.1 M) was prepared by heating 480 mg of sulfur in 150 mL of degassed ODE at 120 °C until complete dissolution. TOP-Se 1 M in TOP was prepared by dissolving 15.8 g of Se powder in 200 mL TOP under magnetic stirring overnight in a glove box.

Synthesis of CdSe cores: CdSe nanocrystals (NCs) were prepared by a procedure slightly modified adapted by Mahler *et al.* [2] from Mohamed *et al.* [3]. A mixture of 2 mL of Cd(oleate)₂ (0.5 M) and 3 mL of ODE was degassed under vacuum at 70 °C during 30 min and heated under argon flow up to 240 °C. A mixture of 1.5 mL of TOP-Se 1 M, 1.5 mL of oleylamine and 1 g of TDPA was heated until complete dissolution then injected and the solution was annealed for 30 seconds at 190 °C, and then immediately cooled down to room temperature. The solution was washed up with 40 mL of ethanol. The solution was centrifuged at 5500 RPM in order to precipitate the TDPA. The nanocrystals were suspended in 20 mL of toluene, washed again in 20 mL of ethanol, and dispersed in 10 mL of hexane. The nanocrystals obtained with this protocol were around 2 nm diameter, and their approximate concentration was 80 μM.

Synthesis of CdS shell on the CdSe cores: For the CdS shell growth on the CdSe cores, a mixture of 3.1 mL of solution of cores dispersed in hexane, 5 mL ODE and 50 mg Cd(myristate)₂ was degassed under vacuum, at 70 °C for 30 minutes, and then put under argon flow. The temperature set value was then increased to 300 °C, and when the temperature reached 100 °C, 1 mL of OLA was injected, followed by a mixture of 8 mL SODE (0.1 M), 1.6 mL Cd(OA)₂ (0.5 M) and 1 mL OLA at an injection rate of first 2 mL/h for 2 mL, then 16 mL/h for the rest of the syringe. Once the injection was finished, a mixture of 0.5 mL OLA and 0.5 mL Cd(OA)₂ 0.1 M diluted in OA was added, and the solution was annealed for 10 minutes at 300 °C. The solution was then cooled down to room temperature and the nanocrystals were washed with ethanol, centrifuged and redispersed in 10 mL hexane.

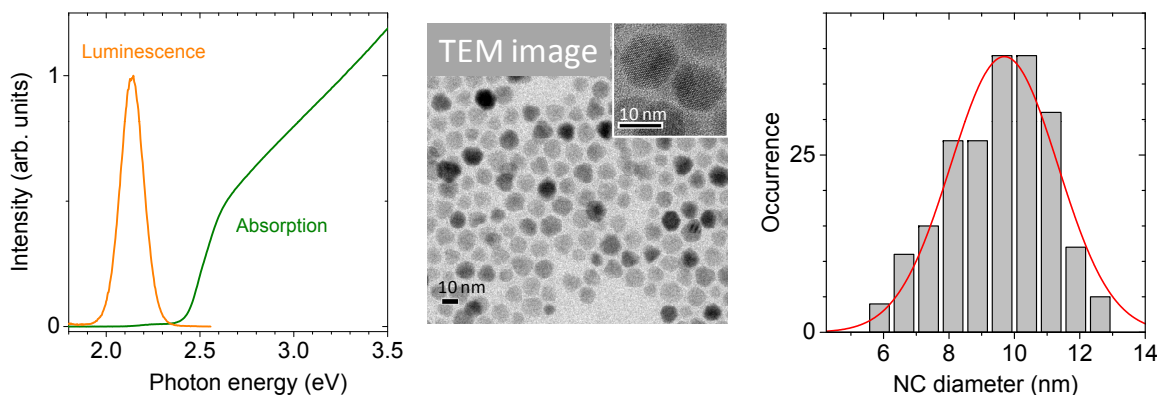


Figure S1. (left) Ensemble absorption and photoluminescence spectra of the CdSe/CdS nanocrystals used in our measurements. (center) Transmission electron microscope image of the CdSe/CdS nanocrystals. (right) Histogram of the NC diameters.

NC characterization: The ensemble absorption spectrum was measured on a Cary 5E UV-visible spectrometer. The ensemble photoluminescence (PL) spectrum was acquired with an Edinburgh Instruments FCS900 spectrometer. Transmission electron microscopy (TEM) images were taken using a TEM JEOL 2010 with field emission electron gun. The results for CdSe/CdS NCs are shown in Figure S1. The NCs show strong PL at 2.14 eV, with a full width at half maximum (FWHM) of 140 meV. From the analysis of the TEM images, we find an statistically averaged diameter of (9.5 ± 1.5) nm.

SYNTHESIS OF CdSe/CdSeS/ZnS NANOPATELETS

Preparation of CdSe nanoplatelets CdSe nanoplatelets (NPs) with an atomically controlled thickness of 4 monolayers were prepared as described in ref [4]. In a 100 mL three neck flask 170 mg (0.3 mmol) of cadmium myristate were introduced along with 12 mg (0.15 mmol) of Se powder and 15 mL of octadecene. The solution was degassed under vacuum for 30 min at room temperature. Under Ar flow, the temperature was set at 240 °C. When the temperature reached 200 °C (the solution is yellow orange at this step), 40 mg (0.15 mmol) of cadmium acetate were quickly added to the solution. Finally the reaction was left for 12 min at 240 °C. Oleic acid (2 mL) were then injected to quench the reaction, and the flask was cooled down to room temperature. The nanoplatelets were precipitated by adding 15 mL of hexane and 15 mL of EtOH. After centrifugation at 6000 rpm for 10 min, the clear supernatant was discarded, and the solid precipitate was re-dissolved in fresh hexane (8 mL). The cleaning procedure was repeated a second time.

Preparation of CdSe/(CdS)₃/(ZnS)₂ nanoplatelets CdSe NPs (500 μL of the solution previously obtained were charged in a 3 mL vial with 0.5 mL of N-methylformamide (NMF) obtaining a biphasic mixture. Then 20 μL from a freshly solution of Na₂S 0.3 M in NMF were added to the biphasic system stirring at room temperature for few minutes. The NPs were thus transferred in the polar NMF bottom phase that turned into orange. The hexane phase was discarded and NPs in NMF were washed twice with hexane to remove residual organic ligand. Then, a mixture of toluene: acetonitrile in a ratio 3:1 is added and NPs were precipitated using centrifugation. The NPs were re-dissolved in 0.5 mL of NMF and 30 μL of Cd(OAc)₂ 0.1 M in NMF were added to complete the first CdS monolayer shell deposition. After stirring of few minutes a room temperature, the NPs were precipitated as described above and re-dissolved in 0.5 mL of NMF. The procedure was repeated two more times for a total of 3 CdS layer deposition. To deposit the two final ZnS shell layers, 20 μL of Na₂S 0.3 M in NMF were added to NPs in NMF and NPs were precipitated using toluene:acetonitrile in a ratio 3:1. After redispersion on NPs in 0.5 mL of NMF, 30 μL of Zn(OAc)₂ 0.1 M in NMF were added and the mixture stirred for few minutes at room temperature. Then, it was precipitated as described above and the procedure was repeated once to complete the shell. The final NPs core/shell were precipitated with toluene and redispersed in 1 mL of hexane adding 100 μL of oleic acid and 50 μL of oleylamine. The excess of organic ligands was washed away by precipitation with EtOH and finally NPs were dissolved in hexane or toluene to be analyzed by transmission electron microscopy (TEM).

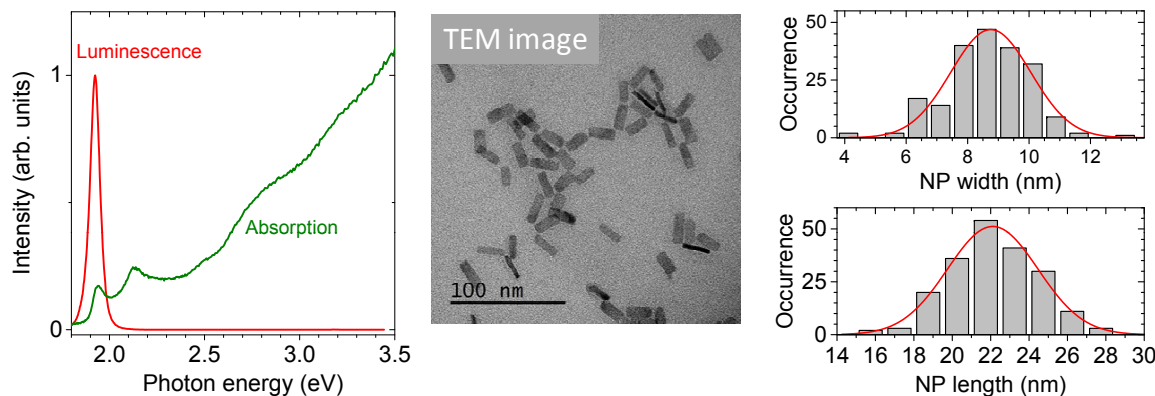


Figure S2. (left) Ensemble absorption and photoluminescence spectra of the CdSe/CdS/ZnS nanoplatelets used in our measurements. (center) Transmission electron microscope image of the CdSe/CdS/ZnS nanoplatelets. (right) Histogram of the NP widths and lengths.

NP characterization: Optical and TEM characterizations of CdSe/CdS/ZnS NPs used in our measurements were performed using the same instruments as for the CdSe/CdS nanocrystals. Figure S2 shows the absorption and PL spectra, as well as a typical TEM image. These NPs show strong emission at 1.925 eV, with a FWHM of 60 meV. From the analysis of the TEM images, we find an average lateral dimensions of (9 ± 1.5) nm \times (22 ± 2) nm. The average height of the NPs is estimated to be (3.5 ± 0.5) nm.

GRAPHENE GROWN BY CHEMICAL VAPOR DEPOSITION

To investigate the distance scaling of the energy transfer rate we made use of graphene grown by low-pressure chemical vapor deposition (LPCVD) on a Cu foil (Alfa Aesar, Item No. 46986, 99.8 %, cut into 6 x 6 cm strips) in a hot wall furnace consisting of a 4 inch fused silica tube [5]. Prior to CVD, the foils were cleaned using a Ni etchant for 5 min and then thoroughly rinsed with DI water. A typical growth process flow is as follows: (1) load the Cu foil, evacuate, heat to 1000 °C, and anneal for 20 min under a 100 sccm H₂ flow (at a pressure of about 70 – 80 mTorr); (2) introduce 30 sccm CH₄ and 30 sccm H₂ for 40 min(60 mTorr); (3) final exposure to CH₄ for 40 min, followed by a cool down of furnace to room temperature in vacuum. A poly(methyl methacrylate) (PMMA) solution (950 K, 4% by volume dissolved in chlorobenzene) was spin-coated onto the top side of the sample followed by baking at 60 °C for 5 min. The Cu under the graphene film was etched using a copper etchant solution and washed with DI water 3 times. The resulting PMMA/graphene film is transferred onto a fused quartz substrate and the PMMA film is dissolved using acetone. In order to remove resist residues and other chemical contaminants from the graphene surface, the samples were heated at 250 °C for 4 hours in a tube furnace in a Ar/H₂ (90/10 % mixture composition) atmosphere.

SAMPLE CHARACTERIZATION BY RAMAN SPECTROSCOPY

Micro-Raman measurements were performed using a home-built setup, with a laser photon energy of 2.33 eV (532 nm) and a power of a few hundred μ W focused onto a diffraction limited spot of $\sim 0.6 \mu\text{m}$ diameter. Figure S3a shows Raman spectra of a mechanically exfoliated graphene monolayer before and after deposition of a thin MgO layer by means of molecular beam epitaxy [6]. The narrow and quasi symmetric lineshape of the 2D mode feature (frequency $\omega_{2D} = 2670 \text{ cm}^{-1}$, FWHM $\Gamma_{2D} = 28 \text{ cm}^{-1}$) is a fingerprint of a graphene monolayer [7]. The bare graphene monolayer exhibits a G-mode frequency (FWHM) of 1586 cm^{-1} (7 cm^{-1}) that are indicative of a slight unintentional doping, on the order of 10^{12} cm^{-2} . This translates into a shift of the Fermi level of less than 200 meV relative to the Dirac point [8].

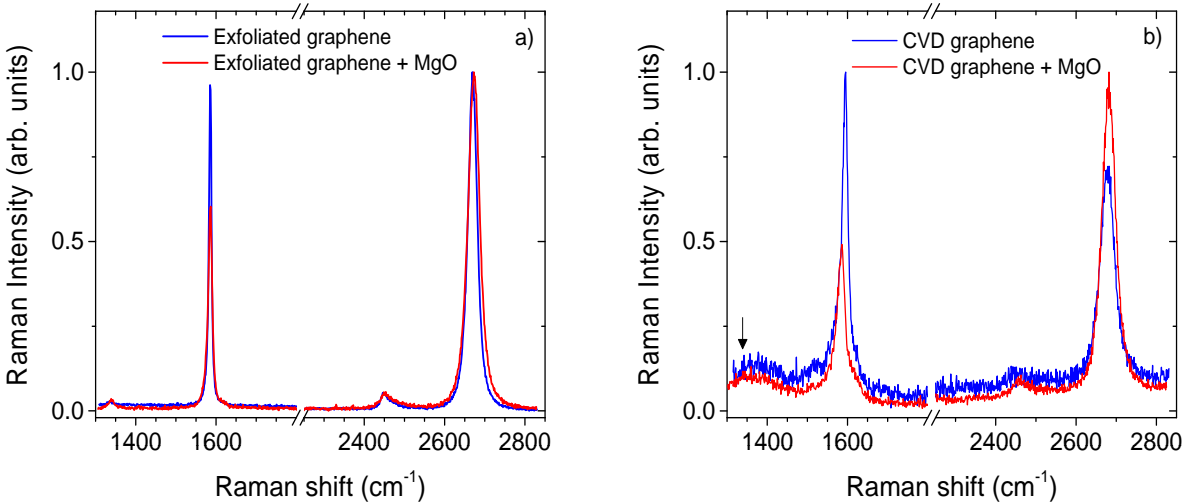


Figure S3. Raman spectra of (a) exfoliated graphene and (b) graphene grown by chemical vapor deposition before and after deposition of a thin MgO film. The arrow in b) indicates the expected position of the D mode feature, which is presumably drowned into the Raman background in these measurements.

After deposition of MgO, we find very similar G and 2D mode frequencies and a slight broadening of the Raman features. The integrated intensity ratio of the defect-induced D mode and the G mode features increases moderately from $I_D/I_G \sim 1\%$ up to $I_D/I_G \sim 3\%$, but remains low (see also Figure S4). We conclude that the deposition of MgO has no major impact on the doping level and is not introducing significant strain as evidenced by the very slight changes in the frequencies. Similar conclusions are reached for a CVD graphene sample transferred on fused silica (see Figure S3b and Figure S5). We observe a slightly stronger background than for measurements on mechanically exfoliated graphene, presumably arising from PMMA residues. CVD graphene also exhibits broader Raman features,

with slightly more scattered frequencies (compare Figure S4 and Figure S5) than for mechanically exfoliated graphene. This likely arises from increased disorder and residual charge inhomogeneity in CVD graphene. Nevertheless, the Raman features are not significantly affected by the deposition of MgO. These results justify the suitability of CVD graphene for our measurements.

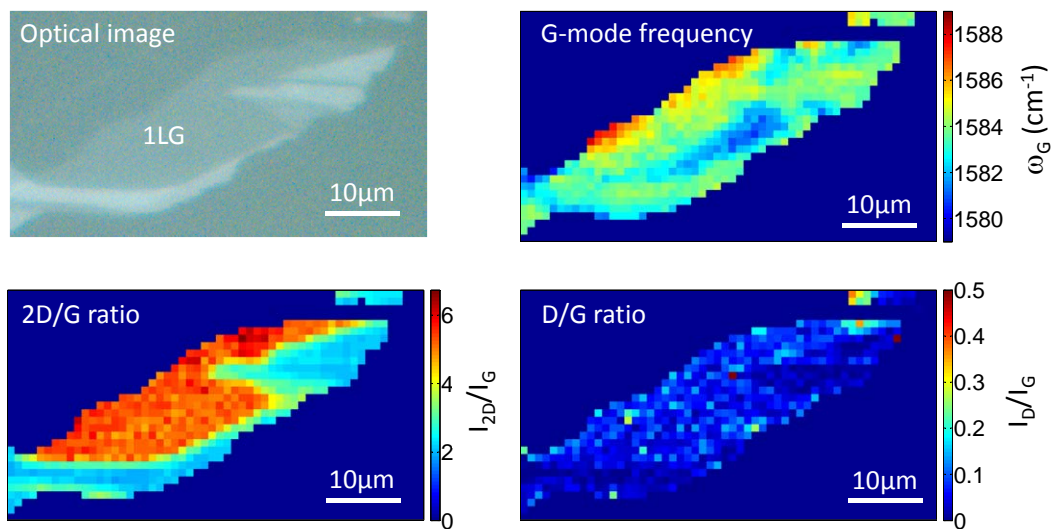


Figure S4. Optical image and spatially resolved Raman study of a mechanically exfoliated graphene sample after deposition of a 2.2 nm thick MgO film.

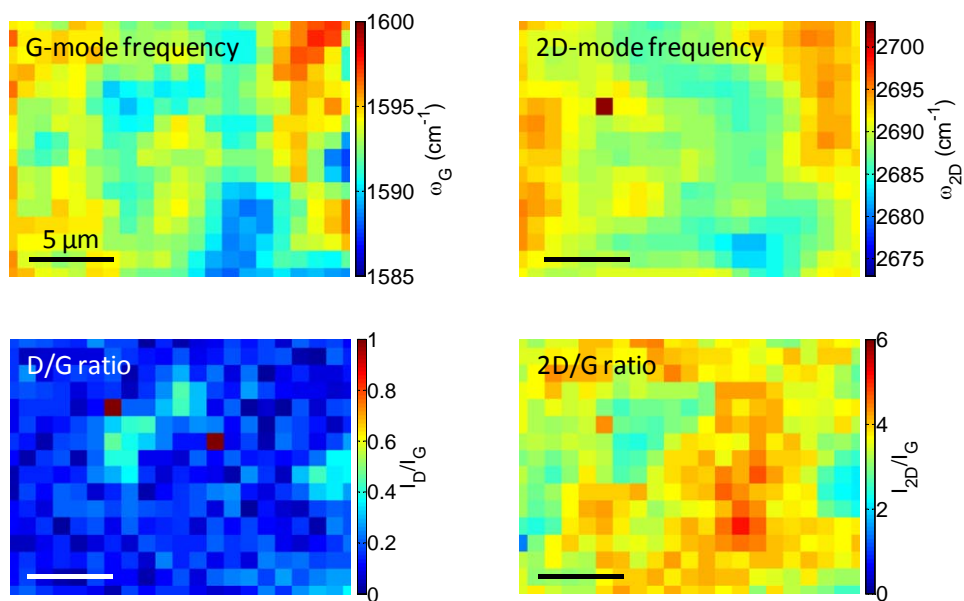


Figure S5. Spatially resolved Raman study of a CVD graphene sample after deposition of a 3.2 nm thick MgO film.

DETERMINATION OF THE DECAY RATES

We define the *calculated* luminescence decay time τ_{calc} as the ratio between the area under the background corrected PL decay curve and its peak value. Applying the latter procedure to our instrument response function (IRF) (see Figures 2 and 3 in the main manuscript) yields a value of $\tau_{\text{calc}}^{\text{IRF}} = 176$ ps. Since the shortest τ_{calc} values measured for NPs on graphene are below 1 ns, the contribution of the IRF to the PL decay has to be taken into account. For this purpose, we have computed τ_{calc} for a set of mono-exponential decays (with a decay time τ_{real}) that have been convoluted with the IRF. The resulting τ_{calc} are plotted against τ_{real} in Figure S6).

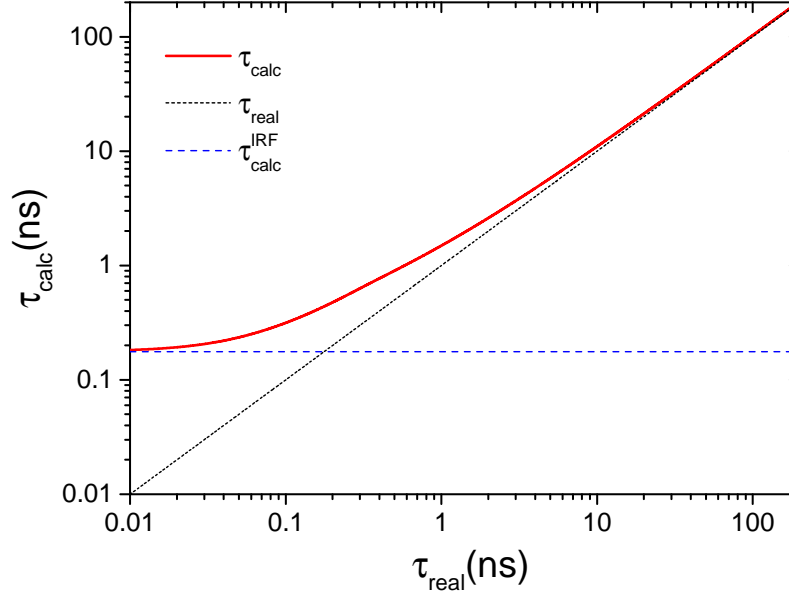


Figure S6. Decay time τ_{calc} numerically computed from the convolution of an exponential decay (decay time τ_{real}) and our instrument response function as a function of τ_{real} .

Then, for each measured PL decay, we calculate τ_{calc} and estimate a value of τ_{real} , by interpolating the calibration curve shown in Figure S6. Obviously, the obtained correction factor assumes a mono-exponential decay. In practice, since τ_{calc} is always significantly greater than $\tau_{\text{calc}}^{\text{IRF}}$, similar correction factors are obtained using other functional forms (bi-exponential decays or stretched exponential decays). We therefore chose to use the procedure described above in order to obtain a general definition of τ_{real} .

In Figures 4 and 5 of the main manuscript, for each thickness of the MgO spacer, we have defined the average decay rate γ as the inverse of the average decay time τ_{real} . We have verified that our conclusions are independent of the method used to define the average PL decay rate.

COMPARISON OF THE DISTANCE DEPENDENT DECAY RATES

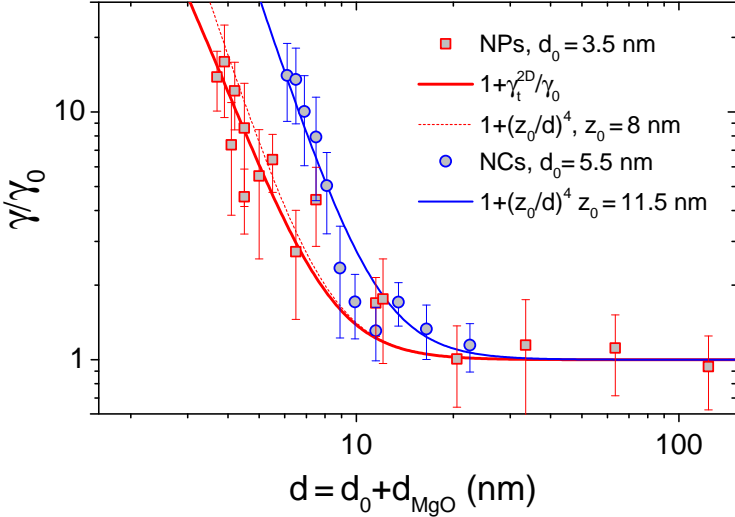


Figure S7. Normalized decay rates measured on individual CdSe/CdS NCs (circles) and CdSe/CdS/ZnS NPs (squares) as a function of the total distance $d = d_0 + d_{\text{MgO}}$ between the nanoemitters and graphene. The solid blue line is computed using Equation 1 in the main text, with $p = 4$ and $z_0 = 11.5$ nm. The solid red line is computed using Equation 3 of the main text, with $\Lambda = 7.5$ nm and a proportionality factor that best fits our results. The dashed red line is computed using Equation 1 in the main text, with $p = 4$ and $z_0 = 8.0$ nm.

Figure S7 compares the normalized distance decay rates γ/γ_0 measured for NCs and NPs (see Figures 4 and 5 of the main manuscript) as a function of the *total* distance $d = d_0 + d^{\text{MgO}}$ between the nanoemitters and graphene. Since the minimal distance d_0 (see main text) is smaller for NPs than for NCs, our results suggest that at a given *total* distance, the RET rate is larger in the case of a zero dimensional NC than for a two-dimensional NP.

* stephane.berciaud@ipcms.unistra.fr

- [1] Yongan Andrew Yang, Huimeng Wu, Kathryn R. Williams, and Y. Charles Cao, "Synthesis of cdse and cdte nanocrystals without precursor injection," *Angewandte Chemie International Edition* **44**, 6712–6715 (2005).
- [2] Benoit Mahler, Piernicola Spinicelli, Stéphanie Buil, Xavier Quelin, Jean-Pierre Hermier, and Benoit Dubertret, "Towards non-blinking colloidal quantumdots," *Nature Materials* **7**, 659–664 (2008).
- [3] Mona B. Mohamed, Dino Tonti, Awos Al-Salman, Abdelkrim Chemseddine, and Majed Chergui, "Synthesis of high quality zinc blende cdse nanocrystals," *The Journal of Physical Chemistry B* **109**, 10533–10537 (2005).
- [4] Sandrine Ithurria and Benoit Dubertret, "Quasi 2D colloidal CdSe platelets with thicknesses controlled at the atomic level," *Journal of the American Chemical Society* **130**, 16504–16505 (2008).
- [5] Xuesong Li, Weiwei Cai, Jinho An, Seyoung Kim, Junghyo Nah, Dongxing Yang, Richard Piner, Aruna Velamakanni, Inha Jung, Emanuel Tutuc, Sanjay K. Banerjee, Luigi Colombo, and Rodney S. Ruoff, "Large-area synthesis of high-quality and uniform graphene films on copper foils," *Science* **324**, 1312–1314 (2009).
- [6] Florian Godel, Emmanuelle Pichonat, Dominique Vignaud, Hicham Majjad, Dominik Metten, Yves Henry, Stéphane Berciaud, Jean-Francois Dayen, and David Halley, "Epitaxy of MgO magnetic tunnel barriers on epitaxial graphene," *Nanotechnology* **24**, 475708 (2013).
- [7] Andrea C. Ferrari and Denis M. Basko, "Raman spectroscopy as a versatile tool for studying the properties of graphene," *Nature Nanotechnology* **8**, 235–246 (2013).
- [8] A. Das, S. Pisana, B. Chakraborty, S. Piscanec, S. K. Saha, U. V. Waghmare, K. S. Novoselov, H. R. Krishnamurthy, A. K. Geim, A. C. Ferrari, and A. K. Sood, "Monitoring dopants by raman scattering in an electrochemically top-gated graphene transistor," *Nature Nanotechnology* **3**, 210–215 (2008).